Origins of $k \cdot p$ errors for [001] GaAs/AlAs **heterostructures**

D. M. Wood[1](*), A. Zunger[1](**) and D. Gershoni[2]

[1] *National Renewable Energy Laboratory - Golden, CO 80401, USA*
[2] *Department of Physics, Technion-Israel Institute of Technology - Haifa, 32000, Israel*

Abstract. – The $k \cdot p$ method + envelope function combination used for semiconductor heterostructures is based on approximations dubious under some conditions. We directly compare 8-band $k \cdot p$ with pseudopotential results for [001] GaAs/AlAs superlattices and quantum wells with all $k \cdot p$ input parameters directly computed from bulk GaAs and AlAs pseudopotential bands. We find generally very good agreement for zone-center hole states within ~ 200 meV of the GaAs valence band maximum, but i) systematic errors deeper in the valence band and ii) qualitative errors for even the lowest conduction bands with appreciable contributions from off-Γ zinc-blende states. We trace these errors to inadequate $k \cdot p$ description of *bulk* GaAs and AlAs band dispersion away from the zone center.

Nanostructures $\gtrsim 100$Å in size were until recently [1] beyond reach of the atomistic electronic structure methods used for bulk crystals, *i.e. direct* solution of the Schrödinger equation

$$\left[-\frac{\hbar^2}{2m}\nabla^2 + \sum_{i,\mathbf{R}_i} v_i(\mathbf{r} - \mathbf{R}_i) \right]\psi(\mathbf{r}) = \varepsilon\,\psi(\mathbf{r}), \tag{1}$$

with the crystal potential $V(\mathbf{r})$ here written as a superposition of screened atomic pseudopotentials v_i for atom species i. The spectroscopy of A/B heterostructures was instead interpreted [2] using an approach so common we term it the 'standard model' (SM): the $k \cdot p$ method combined with the envelope function approximation (EFA). Although the SM has been eminently successful [3], even for ultrathin systems [4], approximations on which it is based compromise its description of heterostructures. Their impact has been partially masked by fitting of its parameters to experimental data, as described below. On general grounds one expects the SM to fail for short-period superlattices but would like to know *when* (for what thicknesses) and *how* (for which states) it fails. While detailed analyses of potential

---

pitfalls of the SM have appeared [5], the SM cannot assess its own validity. Evaluations of actual SM errors via non-SM methods, *e.g.* tight-binding [6], generally used input data (*e.g.* effective masses) from different sources and did not necessarily reflect SM deficiencies. Only by comparing direct solutions of the fully atomistic Schrödinger equation as in eq. (1) can such errors be systematically assessed. This approach is free of approximations made in the standard model, includes full-zone dispersion of all bands, and can predict complete Bloch wave functions. We use [001] $(AlAs)_n(GaAs)_n$ superlattices for $n \leq 20$ and $(GaAs)_n/AlAs$ quantum wells to test the standard model against a direct pseudopotential approach (eq. (1)), with the former's input parameters computed from the latter to guarantee meaningful comparison. We trace systematic errors in the SM for *heterostructures* to inadequate description of dispersion of *bulk* bands in the Brillouin zone region where coupling to off-Γ states is important.

For periodic systems the cell-periodic part u of the Bloch function $\psi_{n\mathbf{k}} = \exp[i\mathbf{k} \cdot \mathbf{r}] u_{n\mathbf{k}}(\mathbf{r})$ may be expanded [7] about a reference point $\mathbf{k}_0$:

$$u_{n\mathbf{k}}(\mathbf{r}) = \sum_{n'}^{N} b_{n'} \, u_{n'\mathbf{k}_0}(\mathbf{r}). \tag{2}$$

Choosing $\mathbf{k}_0 \equiv \Gamma$, the $u_{n\mathbf{k}}(\mathbf{r})$ obey [8]

$$\sum_{n'}^{N} \left\{ \left[\varepsilon_n(\Gamma) - \varepsilon_n(\mathbf{k}) + \frac{\hbar^2 k^2}{2m} \right] \delta_{n,n'} + \frac{\hbar}{m} \mathbf{k} \cdot \mathbf{p}_{n,n'} \right\} b_{n'} = 0; \tag{3}$$

the effects of the microscopic crystal potential are now encoded in the $\mathbf{p}_{n,n'} \equiv \langle u_{n\Gamma} | \hat{\mathbf{p}} | u_{n'\Gamma} \rangle$. Diagonalized with large enough N, eq. (3) would predict *full* (non-parabolic) bands throughout the zone, equivalent to direct solution of the Schrödinger equation for Bloch electrons [9]. The standard model [8], instead uses: i) *Degenerate perturbation theory:* For *bulk* semiconductors, the three valence states degenerate at Γ are usually augmented by the first conduction state. Including spin-orbit defines the 8-band $k \cdot p$ model used below; ii) *Fitting:* The small N values ($\lesssim 20$) in eq. (3) used in most $k \cdot p$ calculations poorly describe band dispersion away from Γ if the $\{ \mathbf{p}_{n,n'} \}$ are actually computed from exact Bloch states $u_{n\Gamma}(\mathbf{r})$. The SM uses instead 'effective' matrix elements found [10] from measured gaps and band effective masses at Γ, mitigating the errors of i); iii) *Envelope functions:* To treat A/B *heterostructures*, the standard model generally uses the Luttinger-Kohn formalism [7] for response of a homogeneous crystal to a weak, *slowly-varying* external perturbation. The wave function in, *e.g.*, material A, takes the form

$$\psi(\mathbf{r}) = \sum_{n=1}^{N} F_n^A(\mathbf{r}) \, u_{n\Gamma}^A(\mathbf{r}), \tag{4}$$

where the $F_n^A(\mathbf{r})$ are 'envelope functions'. The $\{ u_{n,\Gamma} \}$ formally differ in A and B but virtually all EFA's assume the *same* set in *both* except insofar as they affect boundary conditions, via materials properties (*e.g.*, gaps) which differ in A and B. Winkler and Rössler [11] have developed an alternate approach for solving the multiband problem.

Direct solution of eq. (1) makes unnecessary all the approximations above. To compare on an equal footing this 'direct' approach with the 'standard model', 1) We use recent [12] empirical pseudopotentials $v_i(\mathbf{r})$ (including spin-orbit) in eq. (1) to compute band structures for *bulk* zinc-blende (ZB) GaAs and AlAs; the small GaAs/AlAs lattice mismatch is neglected. These pseudopotentials fit to measured band structures of GaAs and AlAs (so that LDA errors do not appear), also closely reproduce important symmetry-related trends in short-period superlattices. 2) We then equate numerically computed effective masses to their formal
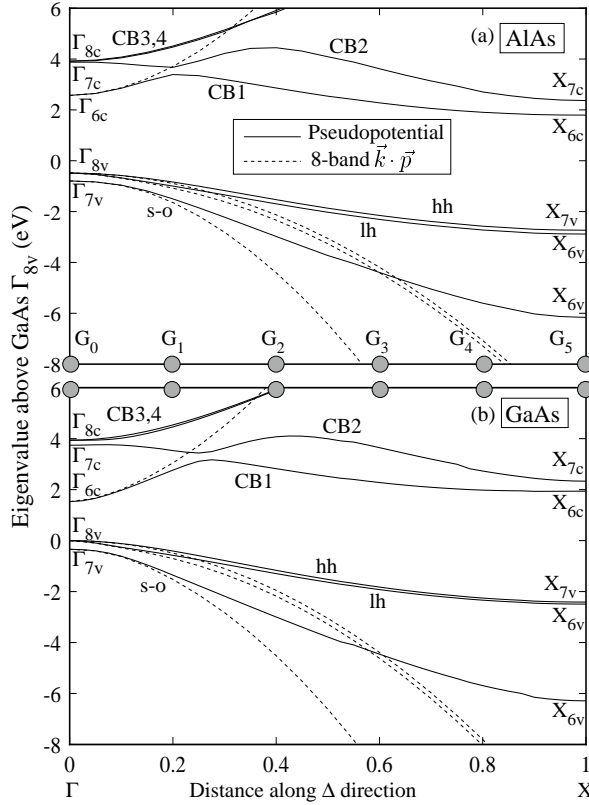
Fig. 1. – AlAs and GaAs near-edge bands between Γ and X ([001] direction). Relativistic labels at Γ and X and conventional names for valence bands are used. Gray circles show points which for [001] $(\text{AlAs})_5(\text{GaAs})_5$ fold to the SL zone center.

expressions [10] in the 8×8 Kane model to extract [13] Luttinger parameters and all relevant matrix elements of eq. (3). 3) We use these as input to $k \cdot p + \text{EFA}$ calculations for [001] GaAs/AlAs superlattices and quantum wells and compare results with direct solutions of eq. (1) for the same structures. The direct 'all band pseudopotential' (ABP) calculations use a conjugate gradient program with a plane wave basis and a 5 Ry kinetic energy cut-off. 'Standard model' (SM) calculations use the 8×8 $k \cdot p + \text{EFA}$ formulation of Baraff and Gershoni [10]. Envelope functions are expanded in 75 Fourier components along the unit cell.

The procedure above permits clean evaluation of approximations made in the 'standard model'. Figure 1 contrasts pseudopotential and $k \cdot p$ bands for *bulk* AlAs and GaAs. For GaAs, $k \cdot p$ and pseudopotential bands agree to within 50 meV only up to 12%, 18%, 14%, and 14% of the distance toward X for the electron (CB1) heavy hole (hh), light hole (lh), and split-off (s-o) bands, respectively. The SM GaAs X_{6c} conduction state is 26 eV higher than the direct pseudopotential value. This gross error in the *bulk* is important for heterostructures since zinc-blende X states fold to the zone center and interact with zinc-blende Γ-derived states. Since the (pseudopotential) GaAs X_{6c}-Γ_{6c} conduction band splitting is only 0.4 eV this interaction is strong, but in the SM is unphysically negligible because the X_{6c} state is 26 eV too high. Superlattice conduction bands in the SM will thus always be spuriously
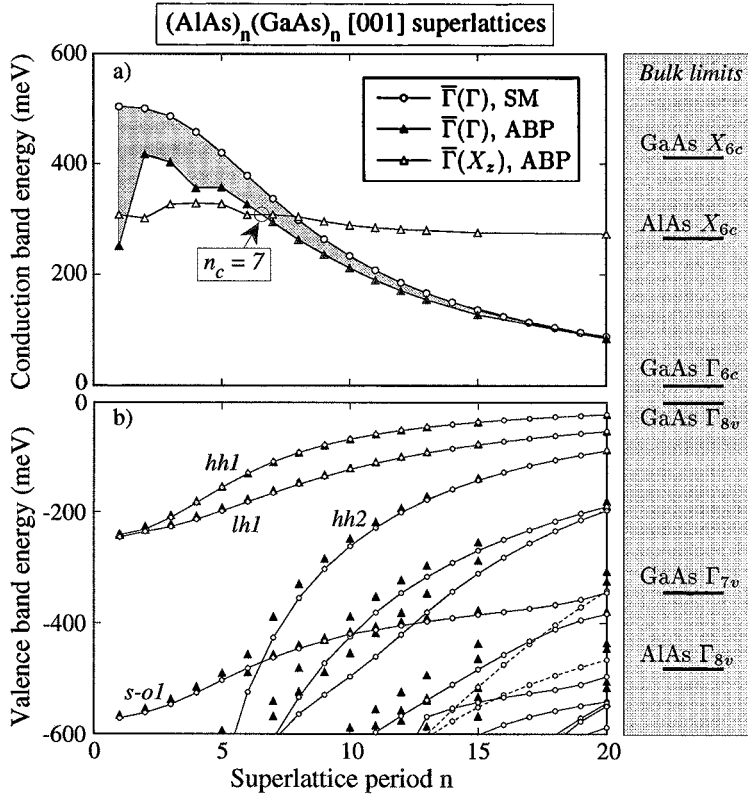
Fig. 2. – Band energies for [001] $(AlAs)_n(GaAs)_n$ superlattices; n_c indicates point of transition from indirect to direct gap system. Overbars indicate SL states which derive mainly from the ZB state in parentheses. Bulk ABP AlAs and GaAs band energies are given at right; the energy zero for a) and b) are bulk GaAs Γ_{6c} and Γ_{8v} states, respectively. Dashed lines show band connectivity near crossings, since Γ-X mixing is practically omitted.

Γ-like [14]. While the SM X_{7v} GaAs valence state is almost 10 eV too low with respect to the pseudopotential value, the resulting error for heterostructure states is small because the pseudopotential $X_{7v} - \Gamma_{8v}$ valence band splitting is large (2.4 eV), so that interaction between heterostructure Γ- and X-derived valence states which fold to the heterostructure zone center is relatively weak.

Figure 2 compares zone-center ABP and SM band energies for [001] $(AlAs)_n(GaAs)_n$ superlattices (SL) as a function of n. We label SL states via an overbar, with the ZB Brillouin zone point from which they derive in parentheses. $\overline{\Gamma}(\Gamma)$ states derive principally from ZB Γ states, while $\overline{\Gamma}(X_z)$ states derive mostly from folded-in zinc-blende X_z states. Only the lowest $\overline{\Gamma}(\Gamma)$ and $\overline{\Gamma}(X_z)$ conduction and near-edge valence bands are shown. The extremely high energy of the SM bulk GaAs X_{6c} state (fig. 1) has important consequences: i) several additional folded-in $\overline{\Gamma}(\Delta_{6c})$ ABP conduction states (not shown) in this energy window are completely missing in the SM; ii) the SM thus misses the transition evident in ABP results (circle in a)) from $\overline{\Gamma}(X_z)$ to $\overline{\Gamma}(\Gamma_{6c})$ as the lowest conduction band; iii) non-monotonicity in the ABP $\overline{\Gamma}(\Gamma)$ conduction band for small n (also present for other points in the SL zone [13] and in first-principles calculations [15]) is absent in the SM, which iv) also overestimates its energy (shading in panel a)). For *valence bands*, i) for states with a binding energy $\lesssim 200$ meV, SM and ABP agree very well, though ii) deeper into the valence band, SM curves reproduce
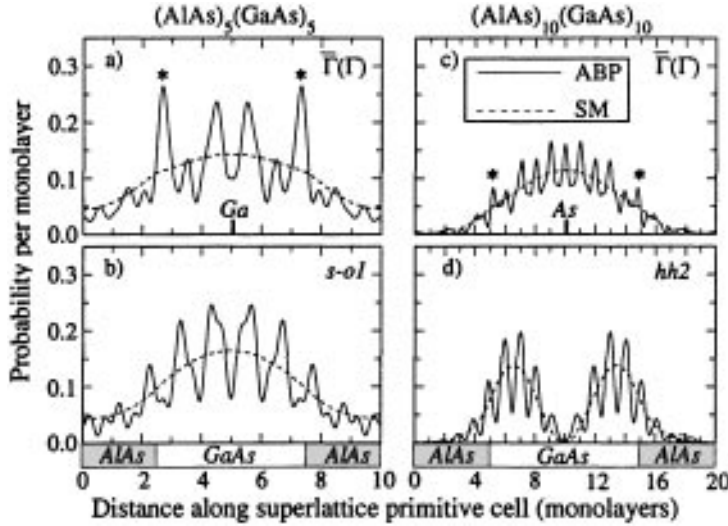
Fig. 3. – Square moduli of planar-averaged ABP Bloch states and SM envelope functions for $\overline{\Gamma}(\Gamma)$ electron state and third hole state at $\overline{\Gamma}$ for $n = 5$ and $n = 10$ SL. Odd (even) n superlattices have inversion symmetry about planes containing Ga (As) atoms. Note peaks on GaAs side of interfaces for electron states (asterisks).

ABP trends but place them *too deep* in energy; iii) for systems lacking inversion symmetry, lifting of the spin degeneracy away from the zone center is permitted in some directions. This spin splitting —absent in the SM— is significant ($\gtrsim 30$ meV for the first heavy-hole state for $\frac{q_\perp a}{2\pi} > 0.1$) for 'in-plane' dispersion in ABP calculations. SM band dispersion (not shown) agrees with ABP results only relatively near the SL zone center [13]. For $n = 5$, ABP values of $m_\parallel/m_\perp$ at $\overline{\Gamma}$ are, *e.g.*, $\simeq 3.4$ for the hh1 state and $\simeq 0.95$ for the $\overline{\Gamma}(\Gamma_{6c})$ electron state, while SM values are 4.4 and 1.3, respectively; the anisotropy of effective masses is thus exaggerated within the SM. $(GaAs)_n/AlAs$ ($1 \le n \le 10$) quantum wells show [13] $n_c \simeq 9$ (cf. fig. 2), differences in valence band dispersion, and $1/n^2$ $\overline{\Gamma}(\Gamma)$ conduction band behavior to smaller n than for superlattices (fig. 2).

Figure 3 contrasts square moduli of ABP wave functions (full lines) averaged over transverse dimensions of the primitive cell to facilitate comparisons with SM envelope functions (dashed lines), for the $\overline{\Gamma}(\Gamma)$ electron state and the third hole state at $\overline{\Gamma}$. Envelope functions for states whose energy (fig. 2) is well described by the SM closely average inner and outer envelopes of Bloch states. The $n = 5$ $\overline{\Gamma}(\Gamma)$ ABP electron wave function shows interfacial peaks absent in the SM.

Projections of SL states onto zinc-blende states provide insight into why and where the SM fails. [001] $(AlAs)_n(GaAs)_n$ superlattice states at $\overline{\Gamma}$ derive from ZB states at the SL reciprocal lattice vectors $G_j = \frac{2\pi j}{na}$ for $j = 0, 1, 2, \ldots, n$ along the [001] Γ-X (Δ) line. We may thus expand a $\overline{\Gamma}$ SL state in a complete set of ZB Bloch states at these G_j:

$$|\psi_{\overline{\Gamma}}^{\mathrm{SL}}\rangle = \sum_s^\infty \sum_{G_j = \Gamma}^X \alpha_{s,G_j} |\psi_{s,G_j}^{\mathrm{ZB}}\rangle; \tag{5}$$

the $G_{j \neq 0}$ (gray circles for $(AlAs)_5(GaAs)_5$ in fig. 1) fold to $\overline{\Gamma}$ in the SL geometry. The projection of a specified SL state onto zinc-blende band s at G_j is thus $P_{sG_j} \equiv |\langle\psi_{\overline{\Gamma}}^{\mathrm{SL}}|\psi_{s,G_j}^{\mathrm{ZB}}\rangle|^2 =$

TABLE I. – *Projections P_{sG_j} of ABP near-edge* (GaAs)$_5$(AlAs)$_5$ *states at $\overline{\Gamma}$ ('State') onto GaAs band s labeled 'On' at the $G_j = \frac{2\pi j}{5a}$, and net projection P_s on band s. G_0 and G_5 correspond to ZB Γ and X points, respectively.*

State	On	G_0	G_1	G_2	G_3	G_4	G_5	P_s
$\overline{\Gamma}(\Gamma)$	CB1	0.80	0.08	0	0.05	0.02	0	0.94
$\overline{\Gamma}(X_z)$	CB1	0	0	0.00	0.00	0.03	0.95	0.99
'hh1'	hh	0.84	0.15	0.00	0.00	0	0	1.00
'lh1'	lh	0.93	0.06	0	0	0	0	0.98
's-o1'	s-o	0.80	0.01	0	0	0	0	0.81
'hh2-a'	hh	0	0.89	0.04	0	0	0	0.93
'hh2-b'	hh	0.14	0.81	0.02	0.00	0	0	0.97
'lh2-a'	lh	0	0.93	0.02	0.	0	0	0.95
'lh2-b'	lh	0.04	0.78	0.01	0	0	0	0.83

$= |\alpha_{s,G_j}|^2$. The net contribution $P_s \equiv \sum_{j=0}^{n} P_{sG_j}$ measures how completely the SL state derives from ZB band s. Similarly, the quantity $P \equiv \sum_{s=1}^{N_b} P_s$ measures how nearly the finite set of N_b zinc-blende bands used is 'complete' ($P \equiv 1$), *i.e.* adequately describes the specified SL state.

For near-edge ABP (AlAs)$_5$(GaAs)$_5$ superlattice states table I shows the projections P_{sG_j} onto the (spin-split) first conduction band CB1 and hh, lh, and s-o valence bands ([1]) —the *same set* used by the 8×8 Kane model. We see that i) superlattice hh1, lh1, and s-o1 states derive mostly from the ZB Γ point (G_0), hh2 and lh2 states mostly from G_1, etc. ii) hh1, lh1, and s-o1 SL states, for example, have significant but monotonically *decreasing* contributions from $G_j \neq 0$, since GaAs valence bands disperse monotonically from Γ (fig. 1b)); iii) the $\overline{\Gamma}(\Gamma)$ conduction state has only a $\simeq 80\%$ projection on the GaAs Γ-point (G_0), with contributions $\sim 20\%$ as large from $G_j \neq G_5$ which depend non-monotonically on j, reflecting the dispersion (fig. 1) of the GaAs CB1 band. We have also evaluated (not shown) P_s, describing *mixing* of different zinc-blende bands in a SL state, and P, measuring basis set *completeness*. For the two SL conduction states in table I the CB1 and CB2 bands of fig. 1 are quasi-complete, *i.e.* $1 - P < 0.004$. *Only* the $\overline{\Gamma}(\Gamma)$ state —ostensibly described by the SM— has an appreciable ($P_s \sim 5.3\%$) contribution from a state (s=CB2) *outside* the set used in the 8-band $k \cdot p$ approach. For SL valence states there is appreciable mixing of ZB states only for s-o1 and deeper valence states, and the hh, lh, s-o set is also quasi-complete.

This shows that *provided* their dispersion is accurately described (as for ABP bands in fig. 1), a *small* number of near-edge zinc-blende bands suffice, in terms of projections, to quantitatively describe SL states. If so, why is the SM unsatisfactory for SL conduction and deep hole bands (figs. 2, 3)? Superlattice hh1, lh1, and s-o1 *hole* bands, which derive mostly from the zinc-blende $G_0 (\equiv \Gamma)$ point, will be *well* described by the standard model since $k \cdot p$ bands are fit there (fig. 1). Deeper SL hole bands (hh2, lh2, *etc.*) derive mostly (table I) from $G_k \neq \Gamma$ points *outside* the quadratic region of good ABP/SM agreement (fig. 1) and will be found *too deep* in the valence band (fig. 2). Since the quadratic region is largest for the GaAs hh band, however, the SM tracks the ABP hh2 band quite well for most n in fig. 2. For the $\overline{\Gamma}(\Gamma)$ *conduction* band, however, contributions from $G_j \neq \Gamma$ (where SM values are too

---

([1]) Due to the great similarity of GaAs and AlAs Bloch states, projections would be very similar had AlAs states been used.

high in energy: fig. 1) are important (table I) and SM predictions *must* be too high (fig. 2) until the shortest G_j move into the CB1 quadratic region. As the period n increases, points along the zinc-blende Δ direction which fold to $\overline{\Gamma}$ move into the region where $k \cdot p$ adequately represents the bulk zinc-blende band structures and all near-edge superlattice states will be well described by the 'standard model'.

We have thus traced errors in the $k \cdot p + $ EFA approach to poor $k \cdot p$ description of dispersion of *bulk* bands which are mixed in heterostructure states. The 8-band $k \cdot p$ approach correctly focuses on four spin-split *bands*, but fails to keep enough (N in eq. (3)) zone-center *states* to adequately describe their dispersion for thin heterostructures. For $Ga_xIn_{1-x}P$ ordered alloys [16] zinc-blende states along the [111] Γ-L direction fold and couple, so the SMs inadequate description of the bulk L point will cause errors similar to those for [001] superlattices. The central issue is not the heterostructure thickness *per se*, but whether off-Γ bulk states poorly described by the 'standard model' are significantly mixed (as determined by the proximity in energy of bulk zinc-blende L, Γ, and X states) in heterostructure bands.

$$***$$

REFERENCES

[1] WANG L.-W. and ZUNGER A., *J. Phys. Chem.*, **98** (1994) 2158; *Phys. Rev. Lett.*, **73** (1994) 1039; *J. Chem. Phys.*, **100** (1994) 2394; MÄDER K. M., WANG L.-W. and ZUNGER A., *Phys. Rev. Lett.*, **74** (1995) 2555.

[2] FASOL G., FASOLINO A. and LUGLI P. (Editors), *Spectroscopy of Semiconductor Microstructures*, *NATO ASI Ser. B.*, Vol. **206** (Plenum Press, New York, N.Y.) 1989.

[3] See, *e.g.*, BASTARD G., BRUM J. A. and FERREIRA R., in *Solid State Physics*, edited by D. TURNBULL and H. EHRENREICH, Vol. **44** (Academic, New York, N.Y.) 1991, p. 229.

[4] See, *e.g.*, ALONSO M.-I., ILG M. and PLOOG K. H., *Phys. Rev. B*, **50** (1994) 1628.

[5] BURT M. G., *J. Phys. Condens. Matter*, **4** (1992) 6651.

[6] SMITH D. L. and MAILHIOT C., *Rev. Mod. Phys.*, **62** (1990) 173.

[7] LUTTINGER J. M. and KOHN W., *Phys. Rev.*, **97** (1955) 869.

[8] KANE E. O., in *Handbook on Semiconductors*, edited by T. S. MOSS, vol. 1 (North Holland, Amsterdam) 1982 Chapt. 4A, pp. 193-217.

[9] CARDONA M. and POLLAK F. H., *Phys. Rev.*, **142** (1966) 530; CARDONA M., CHRISTENSEN N. E. and FASOL G., *Phys. Rev. B*, **38** (1988) 1806.

[10] BARAFF G. A. and GERSHONI D., *Phys. Rev. B*, **43** (1991) 4011. See also GERSHONI D., HENRY C. H. and BARAFF G. A., *IEEE J. Quantum Electron.*, **29** (1993) 2433.

[11] WINKLER R. W. and RÖSSLER U., *Phys. Rev. B*, **48** (1993) 8918.

[12] MÄDER K. A. and ZUNGER A., *Phys. Rev. B*, **50** (1995) 17393.

[13] WOOD D. M. and ZUNGER A., *Phys. Rev. B*, **53**, 15 March 1996.

[14] EDWARDS G. and INKSON J. C., *Solid State Commun.*, **89** (1994) 595 review Γ-X *mixing in heterostructures and other deficiencies of the* EFA.

[15] WEI S.-H. and ZUNGER A., *J. Appl. Phys.*, **63** (1988) 5794.

[16] FRANCESCHETTI A., WEI S.-H. and ZUNGER A., *Phys. Rev. B*, **52** (1995) 13992.